Biomorphological scaling laws from convectively accelerated streams

Biomorphological scaling laws from convectively accelerated streams

G. Calvani[1,2], P. Perona[2], C. Schick[2] and L. Solari[1]

[1]Department of Civil and Environmental Engineering, University of Florence, Florence, Italy

[2]Institute for Infrastructure and Environment, School of Engineering, The University of Edinburgh, United Kingdom

Abstract

Worldwide convectively accelerated streams flowing into downstream-narrowing river sections show that riverbed vegetation growing on alluvial sediment bars gradually disappears forming a front beyond which vegetation is absent. We revise a recent analytical model able to predict the position of the vegetation front. The model was developed considering the steady state approximation of 1-D eco-morphodynamics equations. While the model was tested against flume experiments, its extension and application to the field is not trivial as it requires the definition of proper scaling laws governing the observed phenomenon. In this work, we present a procedure to calculate vegetation parameters and flow magnitude governing the equilibrium at the reach scale between hydro-morphological and biological components in rivers with converging boundaries. We collected data from worldwide rivers about sections topography, hydro-geomorphological and riparian vegetation characteristics to perform a statistical analysis aimed to validate the proposed procedure. Results are presented in the form of scaling laws correlating biological parameters of growth and decay from different vegetation species to flood return period and duration, respectively. Such relationships demonstrate the existence of underlying selective processes determining the riparian vegetation both in terms of species and cover. We interpret the selection of vegetation species from ecomorphodynamic processes occurring in convectively accelerated streams as the orchestrated dynamical action of flow, sediment and vegetation characteristics.

Keywords: fluvial processes; riverbed vegetation; biomass selection; flow uprooting; converging channels

Corresponding author: Giulio Calvani, giulio.calvani@unifi.it

1 Introduction

Riparian and in-channel vegetation must be considered not only as either a source of additional drag to fluvial stream [e.g., *Baptist et al.*, 2007; *Nepf*, 2012; *Vargas-Luna et al.*, 2015, among others] or an agent passively affecting sediment transport and morphological processes [e.g., *Zong and Nepf*, 2010; *Vargas-Luna et al.*, 2016, among others], but also to play an active role within the riverine habitat [*Gurnell*, 2014]. Therefore, it is fundamental to take into account the positive and negative feedbacks between hydro-morpho-dynamics and vegetation establishment, growth and decay [*Edmaier et al.*, 2011; *Perona et al.*, 2012], in order to correctly model river evolution, particularly when referring to long-term predictions. Such mutual interactions gathered attention from scientific community only recently [e.g., see the review by *Camporeale et al.*, 2013]. Specifically, the attention to rivers with converging banks begun with the preliminary conceptual model on island formation proposed by *Gurnell and Petts* [2006] whereas *Edmaier et al.* [2015] and *Bywater-Reyes et al.* [2015] pioneered some studies on the removal conditions of vegetation due to flow in laboratory experiments and field campaigns, respectively. The resulting empirical relationships can be used only when referring to the specific vegetation types involved in their studies. Moreover, results of such predictions are affected by errors mainly originated by the lack of knowledge about the dynamical interactions between vegetation and river morphodynamics [*Solari et al.*, 2016]. Additionally, the temporal and spatial scales at which reciprocal feedbacks between river morphodynamics and riparian vegetation occur still remains an open question [*Manners et al.*, 2015]. Recently developed river eco-morphodynamic models attempt to bridge this gap, by taking into account specific equations for vegetation dynamics (i.e., growth and decay): particularly, the growing term is mainly related to plant-species properties (i.e., by neglecting dependence on nutrient availability and water table level, as usually occurs in river corridors [e.g., *Pasquale et al.*, 2014]), whereas coefficients for decay and mortality due to flow uprooting is intrinsically related to both hydraulic conditions and plant root resistance [*Edmaier et al.*, 2011].

To our knowledge, the first analytical approach to describe eco-morphodynamic interactions has been done by *Perona et al.* [2014], who derived a simple 1-D formulation for the river width where vegetation front is expected to occur in channels with converging banks. Results were validated using previously collected data from laboratory experiments [*Perona et al.*, 2012] but never applied to real case studies. As a matter of fact, in straight channels with parallel riverbanks, vegetation development is mainly imposed on

already settled sedimentary emergent patterns, such as bars and islands, [*Corenblit et al.*, 2007; *Gurnell*, 2014], whereas vegetated rivers with converging boundaries show the distinguishable pattern of a vegetated area inside the main channel downstream which plants are likely to be more easily removed (e.g., figure 1(Replaced: ~~-c,f)~~ replaced with: c-f)). In this planform configuration, due to the intrinsic and dynamically active flow-biomass interaction, a distinctive sediment-plant pattern can be commonly found inside the main channel, particularly, a barebed area where pioneer vegetation is *on average* precluded to colonize and establish [*Perona et al.*, 2014]. Because of the narrowing longitudinal width, the stream is convectively forced to accelerate, resulting in increasing velocity and shear stresses which essentially affect local morphodynamics and promote plant uprooting [*Perona et al.*, 2014], thus limiting the longitudinal establishment and growth of vegetation. Here we stress the term "*on average*" to highlight that the position of the vegetation front changes according to flow regime, but its averaged location is set on the long-term period (i.e., years). Indeed, such location depends on the inter-time between flood events and their magnitude. As a matter of fact, vegetation can colonise the area downstream such position during long low-flow or drought period but it is likely to be uprooted during following high floods, whereas upstream region still remains vegetated. Therefore, vegetation front is the result of the mutual interactions between plant and river characteristics, which, at the front, depend on both biological and hydrological time scales.

In this work, we studied the interactions between riverbed vegetation and river morphodynamics at the reach scale by following the approach of *Perona et al.* [2014] for rivers with converging banks. We first validated the formula for the river width where vegetation front is expected by using already collected data about flow discharge, grain size curve, sediment transport and riparian vegetation size and growth rate from 35 natural worldwide rivers (figure 1(Replaced: ~~-a,b)~~ replaced with: a,b)). Then, we used the validated formula to calculate the flow discharge return period and the flow decay coefficients characterizing the vegetation pattern. Lastly, we could correlate biological parameters of growth and decay to hydrological time scales, and, as a result, prove that vegetation plays a fundamental role in defining the equilibrium conditions of a river reach according to the different species.

2 Materials and Methods

Most of the river reaches with converging banks show the existence of a specific cross-section beyond which vegetation is on average precluded to establish, i.e., there exists a front where vegetation vanishes. *Perona et al.* [2014] experimentally showed that this results from the intensifying capacity of flow to uproot vegetation due to increasing velocity in the convergent reach. They theoretically derived a formula to calculate the river width where vegetation front is located by taking into account biomass dynamics, the steady state of the system from a one-dimensional approach, the approximation of rectangular cross section, the equation of *Baptist et al.* [2007] for the bed roughness with non-submerged vegetation and a modified version of Meyer-Peter-Müller relation for bedload transport which accounts for the additional critical Shields stress due to the presence of roots [*Pasquale et al.*, 2011]. The proposed equation reads:

$$b_f = c^{3/4}\ G^{3/8}\ \left(\theta_c + q_s^{2/3}\right)^{3/8}\ \left(\frac{\beta}{\phi_m}\right)^{7/8}\ Q \tag{1}$$

where b_f is the river width where the vegetation front is located, c is the Gauckler-Strickler roughness coefficient, $G = D_{50}\left(\frac{\rho_s}{\rho} - 1\right)$ is a parameter combining median grain size D_{50}, sediment density ρ_s and water density ρ, θ_c is the critical dimensionless Shield stress for the initiation of sediment movement, $q_s = \frac{Q_s}{k\ b}$ is the dimensionless sediment transport per unit width with $k = 8D_{50}\sqrt{G\ g}$, β is a parameter representing the ratio between vegetation decay rate α_d and growth rate α_g, ϕ_m is the maximum carrying capacity and Q is the average flow discharge at the steady state. While the critical dimensionless Shield stress for the incipient sediment transport θ_c should take into account the presence of plants in the vegetated areas [*Pasquale et al.*, 2011], the value for barebed conditions [e.g., *Chiew and Parker*, 1994] can be assumed when dealing with the area near the vegetation front, where vegetation density is negligible ($\phi \approx 0$). Additionally, it is important to highlight that, while hydraulic coefficients, sediment transport parameters, biomass carrying capacity ϕ_m and growth rate α_g can be easily calculated or retrieved from literature, the decay rate α_d, thus β, and the average flow discharge Q are in general difficult to estimate, and therefore often unknown.

The logistic law for the dynamics of vegetation density ϕ can be expressed as [*Camporeale and Ridolfi*, 2006]:

$$\frac{d\phi}{dt} = \alpha_g\ \phi\ (\phi_m - \phi)\ - \alpha_d\ \phi\ Y\ U^2 \tag{2}$$

Therein, α_g is the growth rate, α_d is the decay rate due to flow uprooting, Y is the flow depth and U is the mean flow velocity. We recall that the growth rate α_g depends on species characteristics only (i.e., when water and nutrients are continually available, as expected in riverine habitats), whereas the decay rate α_d is related to both hydraulics and vegetation properties [*Edmaier et al.*, 2011].

If we assume that growth and decay due to flow are separately active, a possible solution to the logistic law (Eq. (2)) is given in figure 2. Accordingly, we hypothesise that, over a total period $t_d + t_g$, the growth and decay terms are active for fractions $\frac{t_g}{t_d+t_g}$ and $\frac{t_d}{t_d+t_g}$, respectively [*Bärenbold et al.*, 2016; *Crouzy et al.*, 2016]. By accounting for the negligible vegetation density at the front (i.e., $\phi \ll \phi_m$) and the steady state of the solution (i.e., $\frac{d}{dt} = 0$), as hypothesised by *Perona et al.* [2014], we modify the logistic law and obtain:

$$\alpha_g \ \phi_m \ \frac{t_g}{t_g + t_d} - \alpha_d \ Y \ U^2 \ \frac{t_d}{t_g + t_d} = 0 \tag{3}$$

where t_g is the time for which vegetation grows and t_d is the time for which vegetation is removed due to uprooting. Without entirely reporting the mathematical derivation, for which we address the reader to *Perona et al.* [2014], here below we propose to use Eq. (3) in order to rewrite Eq. (1) as

$$b_f = c^{3/4} \ G^{3/8} \ \left(\theta_c + q_s^{2/3}\right)^{3/8} \ \left(\frac{\beta}{\phi_m}\right)^{7/8} \ Q_d \ \left(\frac{t_d}{t_g}\right)^{7/8} \tag{4}$$

where Q_d is the *reference* flow discharge governing bio-morphological changes at the reach scale, a sort of formative discharge controlling vegetation establishment, growth and decay. Again, hydro-morphological (i.e., mean grain size and critical Shields number) and biological (i.e., carrying capacity and growth rate) parameters can be easily obtained from literature or quick field campaigns. On the contrary, quantities related to vegetation decay (i.e., α_d) and temporal durations (e.g., t_d and Q) can be obtained by intensive field investigations over long monitoring periods only.

Here we propose a procedure to calculate the vegetation dynamics parameters and overcome the issue. Firstly, we assume that the equilibrium at the reach scale is achieved over a yearly time scale, that is $t_g + t_d = 365$ days. Secondly, as the flood events able to uproot vegetation are rare, we expect $t_d \ll t_g$ (figure 2) and, as a result, it follows $t_g \approx 365$ d. By doing so, we assume the disturbances induced by high floods having a negligible effect on vegetation growth. Now, by comparing Eq. (1) and Eq. (4) and using

the approximation for t_g, it is easy to obtain:

$$Q \cdot 365^{7/8} = Q_d \cdot t_d^{7/8} \tag{5}$$

which represents a relation among the flow discharge at the steady state Q, the *reference* flow discharge Q_d and the decay duration t_d. Lastly, the flow duration curve is involved in the system of equations, to have an additional relation between flow discharge and time.

We started our analysis by retrieving data for hydraulic (historical daily mean flow discharge), sediment (grain size curve and sediment transport rate) and riparian vegetation properties (species, cover percentage, age and dimensions) for rivers showing a reach with converging banks. We could collect data for 19 rivers and a total of 35 reaches (figure 1). Although convergent boundaries is a worldwide ubiquitous pattern (see figure 1) and figure 1 in *Perona et al.* [2014]), we selected river reaches according to the availability of previously collected data. For reaches in the same rivers, for which we could not find specific data on sediment transport and vegetation cover, we used information from the near cross section. Data about flow discharge were collected at the closest measuring station and used to calculate the yearly duration curve of daily mean flow discharges, while grain size curve and sediment transport rate were taken from previous studies (see complete references after Table 2). We used the D_{50} to calculate the coefficient G and the D_{90} to calculate the Gauckler-Strickler coefficient c in Eq. (1). For the riparian vegetation properties, we collected data from previous monitoring studies, particularly concerning species, cover percentage, maturity age and maximum diameter at maturity age (see Table 2 for references about vegetation data). For each river reach, we characterized the vegetation by averaging the parameters of growth rate α_g and carrying capacity ϕ_m of each species, according to cover percentage, as

$$\overline{\phi}_m = \frac{1}{4046.86} \sum_i \frac{C_i}{b_{0,i}} \left(\frac{D_{max}}{0.0254} \right)^{-b_{1,i}} \tag{6}$$

$$\overline{\alpha}_g = \frac{\pi}{4 \cdot 31536000} \sum_i \frac{C_i \; D_{max,i}^2}{t_{max,i}} \tag{7}$$

Therein, C_i is the cover percentage and $D_{max,i}$ is the diameter at maturity age $t_{max,i}$ of the i$-th$ species, being $b_{0,i}$ and $b_{1,i}$ two coefficients related to the family of the plant. Eq. (6) was modified from *Arner et al.* [2001] whereas we derived Eq. (7) by considering the growth rate of each single species to be constant during the whole life-stage (i.e., the maturity age $t_{max,i}$). Then, according to similar properties of the predominant vegetation species and cover, the 35 study reaches were gathered in 8 different groups. Table

1 summarises group properties and river reach characteristics, whereas all the data can be found in Table 2. Lastly, we took measurements of river width at the vegetation front from Google Earth (e.g., figure 1(Replaced: ~~-c-f)~~ replaced with: c-f)). (Added: Particularly, the river width was measured along the perpendicular to main flow direction in bankfull conditions.)

At this point, we have a system of three equations (i.e., (Replaced: ~~Eqs~~ replaced with: Equations) (1), (5) and flow duration curve for each river reach) but four unknowns: the parameter $\beta = \frac{\alpha_d}{\alpha_g}$, the *reference* flow discharge Q_d, the time durations t_d and the flow discharge at the steady state Q. We solve the problem by exploring the space of solutions in terms of the unknown parameter β over a range of values covering 4 orders of magnitude (i.e., from 10^0 to 10^3 $s^2\,m^{-5}$) for each river reach in a group. Once fixed a value of β, the flow discharge at the steady state Q can be calculated by reversing (Replaced: ~~Eq.~~ replaced with: Equation) (1). It is now straightforward to calculate the left-hand side term in (Replaced: ~~Eq.~~ replaced with: Equation) (5). Then, by using the flow duration curve, it is possible to calculate the (t_d, Q_d) couples (right-hand side term in (Replaced: ~~Eq.~~ replaced with: Equation) (5)) that solve the problem. Usually, two pair values appear as solution (the quantity $Q_d \cdot t_d^{7/8}$ has a typical parabolic like shape) and, between them, we select the one with higher Q_d according to the initial hypothesis $t_d \ll t_g$. The procedure is graphically explained in figure 3: the flow duration curve (continuous black line) is multiplied, once, by the quantity $365^{7/8}$ (light gray line) to calculate the left-hand side term and, once, by the corresponding time $t^{7/8}$ (dashed dark gray line) to obtain the right-hand side quantity in (Replaced: ~~Eq.~~ replaced with: Equation) (5).

Flow discharge Q_d and the corresponding time t_d are recorded for all the river reaches in the same group (i.e., similar vegetation cover) and, then, we calculate the standard deviation of the flow duration t_d, for each tested value of the parameter β. Figure 4 shows the clear trend of such standard deviation at varying the parameter β for some groups of river reaches. As a result, it is possible to identify a minimum in the standard deviation, and, as we are dealing with equilibrium conditions, a minimum in a function seems to suggest the presence of scaling laws associated to the predominant vegetation cover. Moreover, we argue that it is unlikely that different river reaches, with different hydraulic conditions and morphological characteristics, can satisfy the predicting relation ((Replaced: ~~Eq.~~ replaced with: Equation) (1)) and show the existence of such minimum in the t_d standard deviation without it being the expression of an underlying fundamental dynamics depend-

190 **Table 1.** Main vegetation properties and river reaches for each group included in the analysis.

Group	Main properties	Species	Cover	ID	River reaches[a]
1	Populus ≥ 64%	Balsam poplar	64%	1	Clearwater 1
		Other willows	33%	2	Clearwater 2
		Sandbar willow	3%	3	Clearwater 3
		Douglas fir.	77%	16	Salmon
		Sandbar willow	23%		
		Plains cottonwood	78%	32	Yellowstone 1
		Russian olive	16%	33	Yellowstone 2
		Sandbar willow	6%	34	Yellowstone 3
				35	Yellowstone 4
2	Populus < 55% Tamarix > 30%	Fremont cottonwood	52%		
		Salt cedar	41%	14	Rio Grande 1
		Russian olive	6%	15	Rio Grande 2
		Sandbar willow	1%		
		Plains cottonwood	42%	17	San Juan 1
		Russian olive	29%	18	San Juan 2
		Salt cedar	29%		
		Salt cedar	43%	19	San Juan 3
		Russian olive	36%	20	San Juan 4
		Plains cottonwood	21%		
3	Salix > 30%	Salt cedar	56%	4	Colorado 1
		Other willows	30%	5	Colorado 2
		Box elder	14%	6	Colorado 3
		Goat willow	66%	7	Endrick
		Common alder	17%	8	Feshie
		Scots pine	17%		
		Sandbar willow	82%	31	Yampa
		Box elder	18%		
4	Eleagnus > 30%	Other willows	60%	11	Little snake 1
		Russian olive	40%	12	Little snake 2
5	Celtis	Netleaf hackberry	100%	23	Snake 1
				24	Snake 2
6	Thuja	Western cedar	79%		
		Box elder	13%	13	NF Clearwater
		Other willows	8%		
		Western cedar	59%		

Group	Main properties	Species	Cover	ID	River reaches[a]
8	Acer, Betula & Picea	Norway spruce	46%	10	Kander
		Scots pine	31%		
		Grey alder	23%		
		Common alder	40%	27	Tay
		Downy birch	40%		
		Scots pine	20%		
		Salt cedar	62%	28	Virgin
		Freemont cottonwood	23%		
		Black willow	15%		
		Water birch	48%	29	Wind 1
		Spruce	36%	30	Wind 2
		Narrowleaf cottonwood	16%		

[a]Numbers, when present, refer to different reaches in the same river

ing on similar vegetation cover. In the end, for a particular vegetation cover (i.e., group of river reaches), we select the value of the parameter β corresponding to the minimum in the t_d standard deviation, the calculated *reference* flow discharge Q_d and its associated flow duration t_d. Lastly, for the river reaches in a group, we calculate an average decay rate $\overline{\alpha}_d = \beta \cdot \overline{\alpha}_g$.

3 Results

We first used the proposed procedure and a dataset of different vegetation cover properties and hydro-morphological characteristics to validate the relation derived by *Perona et al.* [2014]. We explored the space of the unknown parameter β (i.e., the ratio between decay and growth rates) over four orders of magnitude (i.e., from 10^0 to 10^3 $s^2\,m^{-5}$, see figure 4). As a matter of fact, for higher values of the parameter β, either (Replaced: ~~Eq.~~ replaced with: Equation) (1) does not provide any solution or the solution shows very high t_d standard deviation.

As a result, we obtained different values for the parameter β according to the different vegetation properties. We argue that it depends on the interactions among river mor-

phology (i.e., river width), river hydrology (i.e., flow duration curve) and, intrinsically, the characteristic of the vegetation (i.e., species and coverage). We interpret these interactions and the existence of the minimum in the t_d standard deviation as the orchestrated dynamical action of flow and morphological adjustments which together contribute to select vegetation species sharing biomechanics properties that guarantee their survival in such environments.

We used such values of the β parameter to predict the river width at the vegetation front and compare it against the measured one (e.g., figure 1(Replaced: ~~e)~~ replaced with: c)). Figure 5 shows the comparison between measured and calculated river widths at the vegetation front for each tested river reach. For most of the rivers, the error for the calculated width at the vegetation front is within ± 20% bound, resulting in a high value of the correlation coefficient (R^2 = 0.926). We applied the proposed procedure and the previous calculated β parameters to two additional rivers not included in Table 1: the Tagliamento River (see figure 1(Replaced: ~~e,f)~~ replaced with: e,f) [*Gurnell and Petts*, 2006]) and the Maggia River (see Figure 9 in *Perona et al.* [2014]). We found very good agreement between measured and calculated width at the vegetation front for the case study of the Tagliamento River, whereas the agreement is fairly less good for the Maggia River. The altered flow regime due to upstream flow regulation, in the case of the Maggia River, modified the flow duration curve and, as a result, the return period for moderate flood controlling the vegetation growth and decay is affected when compared to that of natural flood events. Similar conclusion was given by *Perona et al.* [2014] as well.

Furthermore, the procedure proposed in this work allows to calculate the flow magnitude Q_d, its percentile (namely t_d) in the flow duration curve and, additionally, its return period (i.e., t_d^{-1}). Eventually, (Replaced: ~~Eq.~~ replaced with: Equation) (5) provides the equivalent steady state flow discharge Q to be involved in (Replaced: ~~Eq.~~ replaced with: Equation) (1). We combined such results in scaling relationships both for the averaged vegetation decay $\overline{\alpha}_d$ and the averaged growth $\overline{\alpha}_g$ rates, with respect to the different hydrological time scales. Consequently, we could correlate the first one to the time t_d, which fairly resembles the duration of a flood event (figure 6). It is well acknowledged, indeed, that only during high flood events vegetation can be uprooted and removed, due to the simultaneous action of flow drag and bed erosion (Type II uprooting according to *Edmaier et al.* [2011]). Figure 6 shows that each vegetation cover has a particular combination of decay rate and temporal scale t_d governing its removal process. For instance, plant species

of Group 2 and 4 (e.g., Tamarix and Eleagnus) are prone to uprooting (i.e., high $\overline{\alpha}_d$) and can be uprooted with shorter t_d temporal scale. On the contrary, plants species of Groups 1 and 5 (e.g., Populus and Celtis) resulted stronger against uprooting (i.e, low $\overline{\alpha}_d$) and require, for instance, deeper bed erosion for their removal during a flood event.

As a result, it turns out that instantaneous uprooting (Type I according to *Edmaier et al.* [2011]) is unlikely to occur in riverine habitats with already established vegetation and certain flood duration is required for morphological changes (i.e., bed erosion) to reduce root anchoring and promote plant uprooting [*Perona and Crouzy*, 2018; *Calvani et al.*, 2019].

Moreover, we could correlate the average growth rate $\overline{\alpha}_g$ to the return period of the flow magnitude Q_d, which represents a reasonable timescale for plants to start colonising, establish and grow on river bare bedforms. The flood return period T was calculated as the reciprocal of the timescale t_d: for the sake of clarity, T is the return period of a daily flow discharge equal to the *reference* flow discharge Q_d.

The results of the correlation are shown in figure 7. Particularly, figure 7 highlights that plants with low growth rate (e.g., Group 5 and 7) can survive in fluvial systems characterised by low flow magnitude Q_d (i.e., short return period T). On the contrary, species with higher growth rate can withstand higher flood events. In this regard, the case of Tamarix species (Group 2) represents a particular case, as this species is recognised to be invasive in many ecosystems and, once established, very hard to removed [e.g., *Sher et al.*, 2002; *Stromberg et al.*, 2007]. In such a way, the results suggest that in a given hydromorphological fluvial system (i.e., once the channel geometry, grain size distribution and hydrological regime are fixed), only some plants species, and within the same species, only mature plants (i.e., old enough to have developed a strong root apparatus) can tackle flood events. We interpreted these biomorphological scaling relationships as the ability for rivers to select vegetation according to their growing and survival properties. On the contrary, such relationships quantify the ability for plants species to withstand convectively increasing specific stream power within the converging channel and the particular hydrological conditions.

4 Discussion

The role of riparian and in-channel vegetation is commonly acknowledged among the factors controlling the morphodynamic evolution of fluvial environments [see *Camporeale et al.*, 2013, for a review]. As the presence of such biological component started to be taken into account in modelling only recently [e.g., *van Oorschot et al.*, 2016], the morphodynamic equilibrium at the reach scale is usually modelled by means of empirical relationships, mostly related to bankfull discharge or other characteristic values [e.g., *Parker et al.*, 2007; *Wilkerson and Parker*, 2010], without explicitly accounting for the presence of vegetation. Figure 8 shows the comparison between the measured width at the vegetation front and the predicted bankfull width using the Lacey's relationship [*Savenije*, 2003] for the steady state flow discharge Q resulting from the performed analysis.

Results are somehow controversial: the bankfull predictor seems to work better in the cases where one can expect vegetation to play a significant role, that is when river width is narrower (i.e., measured b_f lower than 150 m). On the contrary, for wider rivers, the prediction works well with the proposed formulation (see figure 5 for comparison). This suggests that the steady state flow discharge Q in (Replaced: ~~Eq.~~ replaced with: Equation) (1) is representative of bankfull discharge only for narrow fluvial systems (i.e., with $b_f <$ 150m), whereas the vegetation dynamics is governed by higher flow discharges in larger rivers. Similarly, vegetation front is located at the bankfull width in small streams, whereas its location is upstream (i.e., where river width is larger due to the convergent configuration) of the bankfull width correspondent to the flow discharge Q.

Figure 5 shows some predicting errors in the estimation of river width at the vegetation front. Such errors can be ascribed to the simplifications introduced in the model ((Replaced: ~~Eq.~~ replaced with: Equation) (4)), with particular focus on the one-dimensional approach to river geometry and flow. In this regard, (Replaced: ~~for river reaches showing in-channel vegetated bars (see figure 1(Replaced: -c-f) replaced with: c-f)),~~ replaced with: some river reaches included in the analysis show the presence of large-scale bedforms (i.e., central or multiple bars) covered by in-channel vegetation (see figure 1c-f). For such rivers,) it is straightforward to assume the steady state flow discharge Q as a conceptual value only, whereas the *reference* discharge Q_d represents the flow governing the vegetation dynamics. Additionally, the evolution of such large-scale bedforms (Deleted: ~~(see figure 1-c,d))~~is not explicitly taken into account in (Replaced: ~~Eq.~~ replaced with: Equa-

tion) (1) (the model is one-dimensional)(Replaced: ~~but~~ replaced with: . Nevertheless,) their influence on flow can be considered by an appropriate roughness coefficient c. Prediction errors can also be correlated to either measuring errors from Google Earth (although limited to some meters) or the different flow period when pictures were taken (e.g., low or high water stage). Furthermore, in some cases, due to the absence of measuring stations, we used similar data of flow duration curve and vegetation cover for different reaches in the same river, regardless of the distance among them (e.g., reaches 33, 34 and 35 in figure 5). Although we did not identify tributaries from aerial photos, the presence of small streams may lead to downstream alteration in the flow regime.

Analysis results are intrinsically related to the additionally hypothesis made in the proposed procedure. Conversely to t_d for $\overline{\alpha}_d$, we cannot involved t_g as a temporal scale for the growth rate $\overline{\alpha}_g$, as we fixed its value ($t_g \approx$365d). It follows that, according to the flow regime of each particular river, this approximation may lead to errors when, for instance, the bio-morphological equilibrium requires longer time to be achieved. Morphodynamic processes (e.g., width adjustment, bank erosion, bar migration) can delay the achievement of such equilibrium and, in this case, a longer time scale t_g should be taken into account. This should also be considered when dealing with important alterations in the flow regime, both in relation to natural changes due to climate change [e.g., *Stromberg et al.*, 2010; *Rivaes et al.*, 2013] and human interventions due to flow regulation [e.g., *Johnson*, 1997] or dam removal [e.g., *Shafroth et al.*, 2002], and in the vegetation cover, due to alien species colonisation [e.g., *Stromberg et al.*, 2007] or artificial plantations [e.g., *Perry et al.*, 2001]. (Added: It is undisputed that such factors may induced change in the eco-morphodynamic equilibrium at different temporal scales. A river subjected to flow regulation by damming which, for instance, increases the return period of the *reference flow discharge*, will react by showing a narrower b_f in the short term. In other words, the vegetation front moves downstream, because, with a higher return period, plants have longer time to grow and colonise the river bed. However, on the long term, the new return period will result in a different vegetation cover (selection mechanism), as pointed out in Figure 7. Similar considerations can be made in the opposite case.)In this regard, the presence of outliers in figure 6 (Group 6) and in figure 7 (Group 1) can be explained by considering the main species composing the vegetation cover. Group 1 is mainly constituted by river reaches showing *Populus* species in the plant composition: poplars are known for its fast growing ($\overline{\alpha}_g$ in figure 7) and, accordingly, they were artifi-

cially introduced in riverine environments for timber production. Conversely, Group 6 is mainly constituted by reaches showing plants of the genre *Thuja*. Such plants are more typical of swamps and wetlands, rather than riverine habitats, and their low decay rate $\overline{\alpha}_d$ may be related to the rare occurrence of flow uprooting in such environments [*Stewart*, 2009].

5 Conclusions

In this work, we analysed the interactions between river morphodynamics and vegetation properties at the reach scale. We based our analysis on the one-dimensional equations derived by *Perona et al.* [2014] for the river width where vegetation front is located, provided the existence of an ubiquitous pattern in rivers with convergent boundaries. We first proposed a procedure to calculate the biological parameters and hydrological timescales governing such equilibrium at the reach scale. Accordingly, we validated the proposed procedure against data from real rivers on a yearly time scale, accounting for the effective duration of flow removal, and concluded that vegetation front location is predictable and dependent on the vegetation species, thus providing guidance for future river restoration projects. Due to the defined planform configuration, we could point out the implicit interplays among plants species, river morphology and flow duration. As a result, we demonstrate the ability for rivers to select, by hydrodynamic-induced mortality, biomass (i.e., plant species) according to the flow regime (flood event return period and duration) of the river itself. Furthermore, our analysis shows the importance of accounting for vegetation dynamics and its influence on river properties, both in long-term simulations where flow conditions change in time according to time-scale depending on growth rate α_g and at the flood event scale, where vegetation density changes according to α_d: therefore, the choice of time-scale and time-step shall reflect not only hydraulic conditions but also vegetation properties.

Acknowledgments

We thank the Associated Editor and two anonymous reviewers whose comments and suggestions helped to improve the manuscript.

References

Al-Ansari, N., and J. McManus (1979), Fluvial sediments entering the tay estuary: sediment discharge from the river earn, *Scottish Journal of Geology*, *15*(3), 203–216.

Andrews, E. D. (1980), Effective and bankfull discharges of streams in the yampa river basin, colorado and wyoming, *Journal of Hydrology*, *46*(3-4), 311–330.

Andrews, E. D. (1984), Bed-material entrainment and hydraulic geometry of gravel-bed rivers in colorado, *Geological Society of America Bulletin*, *95*(3), 371–378.

Arner, S. L., S. Woudenberg, S. Waters, J. Vissage, C. MacLean, M. Thompson, and M. Hansen (2001), National algorithms for determining stocking class, stand size class, and forest type for forest inventory and analysis plots, *Internal Rep. Newtown Square, PA: US Department of Agriculture, Forest Service, Northeastern Research Station. 10p*.

Ashworth, P. J., and R. I. Ferguson (1989), Size-selective entrainment of bed load in gravel bed streams, *Water Resources Research*, *25*(4), 627–634.

Auble, G. T., J. M. Friedman, P. B. Shafroth, M. F. Merigliano, and M. L. Scott (2012), Woody riparian vegetation near selected streamgages in the western united states, *US Geological Survey Data Series*, *Data series: 708*.

BAFU Data (2017), erhebung von Daten zum Umweltzustand des Bundesamtes für Umwelt; `https://www.bafu.admin.ch/bafu/de/home/zustand/daten/umweltdaten.html`.

BAFU GeoData (2017), verfügbare Geodaten des Bundesamtes für Umwelt; `https://www.bafu.admin.ch/bafu/de/home/zustand/daten/geodaten.html`.

Baptist, M., V. Babovic, J. Rodríguez Uthurburu, M. Keijzer, R. Uittenbogaard, A. Mynett, and A. Verwey (2007), On inducing equations for vegetation resistance, *Journal of Hydraulic Research*, *45*(4), 435–450.

Bärenbold, F., B. Crouzy, and P. Perona (2016), Stability analysis of ecomorphodynamic equations, *Water Resources Research*, *52*(2), 1070–1088.

Bates, C., C. Moore, T. Malthus, J. Mair, and E. Karpouzli (2004), Broad scale mapping of habitats in the firth of tay and eden estuary, scotland, *Scottish Natural Heritage Comissioned Report*, *7*.

Bryant, R. G., and D. J. Gilvear (1999), Quantifying geomorphic and riparian land cover changes either side of a large flood event using airborne remote sensing: River tay, scotland, *Geomorphology*, *29*(3-4), 307–321.

Bywater-Reyes, S., A. C. Wilcox, J. C. Stella, and A. F. Lightbody (2015), Flow and scour constraints on uprooting of pioneer woody seedlings, *Water Resources Research*, *51*(11), 9190–9206.

Calvani, G., S. Francalanci, and L. Solari (2019), A physical model for the uprooting of flexible vegetation on river bars, *Journal of Geophysical Research: Earth Surface*, *124*(4), 1018–1034, doi:10.1029/2018JF004747.

Camporeale, C., and L. Ridolfi (2006), Riparian vegetation distribution induced by river flow variability: A stochastic approach, *Water Resources Research*, *42*(10).

Camporeale, C., E. Perucca, L. Ridolfi, and A. Gurnell (2013), Modeling the interactions between river morphodynamics and riparian vegetation, *Reviews of Geophysics*, *51*(3), 379–414.

Charlton, F., P. Brown, and R. Benson (1978), *The hydraulic geometry of some gravel rivers in Britain*, Hydraulics Research Station, Wallingford (UK).

Chiew, Y.-M., and G. Parker (1994), Incipient sediment motion on non-horizontal slopes, *Journal of Hydraulic Research*, *32*(5), 649–660.

Claessens, H., A. Oosterbaan, P. Savill, and J. Rondeux (2010), A review of the characteristics of black alder (*Alnus glutinosa* (l.) gaertn.) and their implications for silvicultural practices, *Forestry*, *83*(2), 163–175.

Corenblit, D., E. Tabacchi, J. Steiger, and A. M. Gurnell (2007), Reciprocal interactions and adjustments between fluvial landforms and vegetation dynamics in river corridors: a review of complementary approaches, *Earth-Science Reviews*, *84*(1), 56–86.

Crouzy, B., F. Bärenbold, P. DâĂŹOdorico, and P. Perona (2016), Ecomorphodynamic approaches to river anabranching patterns, *Advances in water resources*, *93*, 156–165.

Edmaier, K., P. Burlando, and P. Perona (2011), Mechanisms of vegetation uprooting by flow in alluvial non-cohesive sediment, *Hydrology and Earth System Sciences*, *15*(5), 1615–1627.

Edmaier, K., B. Crouzy, and P. Perona (2015), Experimental characterization of vegetation uprooting by flow, *Journal of Geophysical Research: Biogeosciences*, *120*(9), 1812–1824.

Elliott, J. G., and S. P. Anders (2004), *Summary of sediment data from the Yampa River and Upper Green River basins, Colorado and Utah, 1993-2002*, 5242, US Department of the Interior, US Geological Survey.

Enescu, C., T. H. Durrant, D. de Rigo, and G. Caudullo (2016), *Salix caprea* in europe: distribution, habitat, usage and threats, in *European atlas of forest tree species*, Publications Office of the European Union, Luxembourg (L).

FLO Engineering, I. (1994), Little snake river channel monitoring project, *Tech. Rep. 1994 fall channel monitoring trip*, US Fish and Wildlife Service, National Park Service and Colorado State University.

Gilvear, D., J. Cecil, and H. Parsons (2000), Channel change and vegetation diversity on a low-angle alluvial fan, river feshie, scotland, *Aquatic Conservation: Marine and Freshwater Ecosystems*, *10*(1), 53–71.

Gurnell, A. (2014), Plants as river system engineers, *Earth Surface Processes and Landforms*, *39*(1), 4–25.

Gurnell, A., and G. Petts (2006), Trees as riparian engineers: the Tagliamento River, Italy, *Earth Surface Processes and Landforms*, *31*(12), 1558–1574.

Heins, A., A. Simon, L. Farrugia, and M. Findeisen (2004), Bed-material characteristics of the san juan river and selected tributaries, new mexico: developing protools for stream-bottom deposits, *Tech. Rep. No. 47*, USDA-ARS.

Hoag, J. C. (2005), Simple identification key to common willows, cottonwoods, alder, birch and dogwood of the intermountain west, *Aberdeen (ID): USDA Natural Resources Conservation Service, Aberdeen Plant Materials Center. Riparian/Wetland Project Information Series*, *19*, 16.

Holnbeck, S. R. (2005), *Sediment-transport investigations of the Upper Yellowstone River, Montana, 1999 through 2001: data collection, analysis, and simulation of sediment transport*, US Department of the Interior, US Geological Survey.

Johnson, W. C. (1997), Equilibrium response of riparian vegetation to flow regulation in the platte river, nebraska, *Regulated Rivers: Research & Management: An International Journal Devoted to River Research and Management*, *13*(5), 403–415.

Jud, D. (2009), Eigendynamische flussaufweitungen der kander im gebiet heustrich süd, masters' thesis, EPFL, Losanne (CH).

Little, E. L., and L. A. Viereck (1971), *Atlas of United States trees*, vol. 5, US Dept. of Agriculture, Forest Service, Washington, DC.

Manners, R. B., A. C. Wilcox, L. Kui, A. F. Lightbody, J. C. Stella, and L. S. Sklar (2015), When do plants modify fluvial processes? Plant-hydraulic interactions under variable flow and sediment supply rates, *Journal of Geophysical Research: Earth Sur-*

face, *120*(2), 325–345.

Mueller, E. R., and J. Pitlick (2013), Sediment supply and channel morphology in mountain river systems: 1. relative importance of lithology, topography, and climate, *Journal of Geophysical Research: Earth Surface*, *118*(4), 2325–2342.

Mueller, E. R., J. Pitlick, and J. M. Nelson (2005), Variation in the reference shields stress for bed load transport in gravel-bed streams and rivers, *Water Resources Research*, *41*(4).

National River Flow Archive (2017), `https://nrfa.ceh.ac.uk/`.

Nepf, H. M. (2012), Hydrodynamics of vegetated channels, *Journal of Hydraulic Research*, *50*(3), 262–279.

Novak, S. J. (2006), Hydraulic modelling analysis of the middle rio grande river from cochiti dam to galisteo creek, new mexico, masters' thesis, Colorado State University, Fort Collins, CO (USA).

Parker, G., P. R. Wilcock, C. Paola, W. E. Dietrich, and J. Pitlick (2007), Physical basis for quasi-universal relations describing bankfull hydraulic geometry of single-thread gravel bed rivers, *Journal of Geophysical Research: Earth Surface*, *112*(F4).

Pasquale, N., P. Perona, P. Schneider, J. Shrestha, A. Wombacher, and P. Burlando (2011), Modern comprehensive approach to monitor the morphodynamic evolution of a restored river corridor, *Hydrology and Earth System Sciences*, *15*(4), 1197–1212.

Pasquale, N., P. Perona, R. Francis, and P. Burlando (2014), Above-ground and below-ground Salix dynamics in response to river processes, *Hydrological processes*, *28*(20), 5189–5203.

Perona, P., and B. Crouzy (2018), Resilience of riverbed vegetation to uprooting by flow, *Proc. R. Soc. A*, *474*(2211).

Perona, P., P. Molnar, B. Crouzy, E. Perucca, Z. Jiang, S. McLelland, D. Wüthrich, K. Edmaier, R. Francis, C. Camporeale, et al. (2012), Biomass selection by floods and related timescales: Part 1. experimental observations, *Advances in Water Resources*, *39*, 85–96.

Perona, P., B. Crouzy, S. McLelland, P. Molnar, and C. Camporeale (2014), Ecomorphodynamics of rivers with converging boundaries, *Earth Surface Processes and Landforms*, *39*(12), 1651–1662.

Perry, C. H., R. C. Miller, and K. N. Brooks (2001), Impacts of short-rotation hybrid poplar plantations on regional water yield, *Forest Ecology and Management*, *143*(1-3), 143–151.

519 Piedra, M. M. (2010), Flume investigation of the effects of sub-threshold rising flows on
520 the entrainment of gravel beds, Ph.D. thesis, University of Glasgow, Glasgow (UK).
521 Rivaes, R., P. M. Rodríguez-González, A. Albuquerque, A. N. Pinheiro, G. Egger, and
522 M. T. Ferreira (2013), Riparian vegetation responses to altered flow regimes driven by
523 climate change in mediterranean rivers, *Ecohydrology*, *6*(3), 413–424.
524 Savenije, H. H. (2003), The width of a bankfull channel; lacey's formula explained, *Jour-*
525 *nal of Hydrology*, *276*(1-4), 176–183.
526 Shafroth, P. B., J. M. Friedman, G. T. Auble, M. L. Scott, and J. H. Braatne (2002), Po-
527 tential responses of riparian vegetation to dam removal: dam removal generally causes
528 changes to aspects of the physical environment that influence the establishment and
529 growth of riparian vegetation, *BioScience*, *52*(8), 703–712.
530 Sharma, M., and J. Parton (2007), Height–diameter equations for boreal tree species in on-
531 tario using a mixed-effects modeling approach, *Forest Ecology and Management*, *249*(3),
532 187–198.
533 Sher, A. A., D. L. Marshall, and J. P. Taylor (2002), Establishment patterns of native pop-
534 ulus and salix in the presence of invasive nonnative tamarix, *Ecological applications*,
535 *12*(3), 760–772.
536 Smith, H. Y. (1999), Assessing longevity of ponderosa pine (pinus ponderosa) snags in
537 relation to age, diameter, wood density and pitch content, masters' thesis, University of
538 Montana, Missoula, MT (USA).
539 Solari, L., M. Van Oorschot, B. Belletti, D. Hendriks, M. Rinaldi, and A. Vargas-Luna
540 (2016), Advances on modelling riparian vegetation-hydromorphology interactions, *River*
541 *Research and Applications*, *32*(2), 164–178.
542 Stewart, H. (2009), *Cedar: tree of life to the Northwest Coast Indians*, D & M Publishers.
543 Stromberg, J. C., S. J. Lite, R. Marler, C. Paradzick, P. B. Shafroth, D. Shorrock, J. M.
544 White, and M. S. White (2007), Altered stream-flow regimes and invasive plant species:
545 the tamarix case, *Global Ecology and Biogeography*, *16*(3), 381–393.
546 Stromberg, J. C., S. J. Lite, and M. Dixon (2010), Effects of stream flow patterns on ripar-
547 ian vegetation of a semiarid river: implications for a changing climate, *River Research*
548 *and Applications*, *26*(6), 712–729.
549 van Oorschot, M., M. Kleinhans, G. Geerling, and H. Middelkoop (2016), Distinct pat-
550 terns of interaction between vegetation and morphodynamics, *Earth Surface Processes*
551 *and Landforms*, *41*(6), 791–808.

552 Vargas-Luna, A., A. Crosato, and W. S. Uijttewaal (2015), Effects of vegetation on flow
553 and sediment transport: comparative analyses and validation of predicting models, *Earth*
554 *Surface Processes and Landforms*, *40*(2), 157–176.
555 Vargas-Luna, A., A. Crosato, G. Calvani, and W. S. Uijttewaal (2016), Representing plants
556 as rigid cylinders in experiments and models, *Advances in Water Resources*, *93*, 205–
557 222.
558 Warner, R., and K. Hendrix (1984), *California riparian systems: ecology, conservation,*
559 *and productive management*, University of California Press, Berkeley, CA (USA).
560 Water Data for the Nation (2017), `https://waterdata.usgs.gov/nwis`.
561 Wilkerson, G. V., and G. Parker (2010), Physical basis for quasi-universal relationships
562 describing bankfull hydraulic geometry of sand-bed rivers, *Journal of Hydraulic Engi-*
563 *neering*, *137*(7), 739–753.
564 Zong, L., and H. Nepf (2010), Flow and deposition in and around a finite patch of vegeta-
565 tion, *Geomorphology*, *116*(3), 363–372.

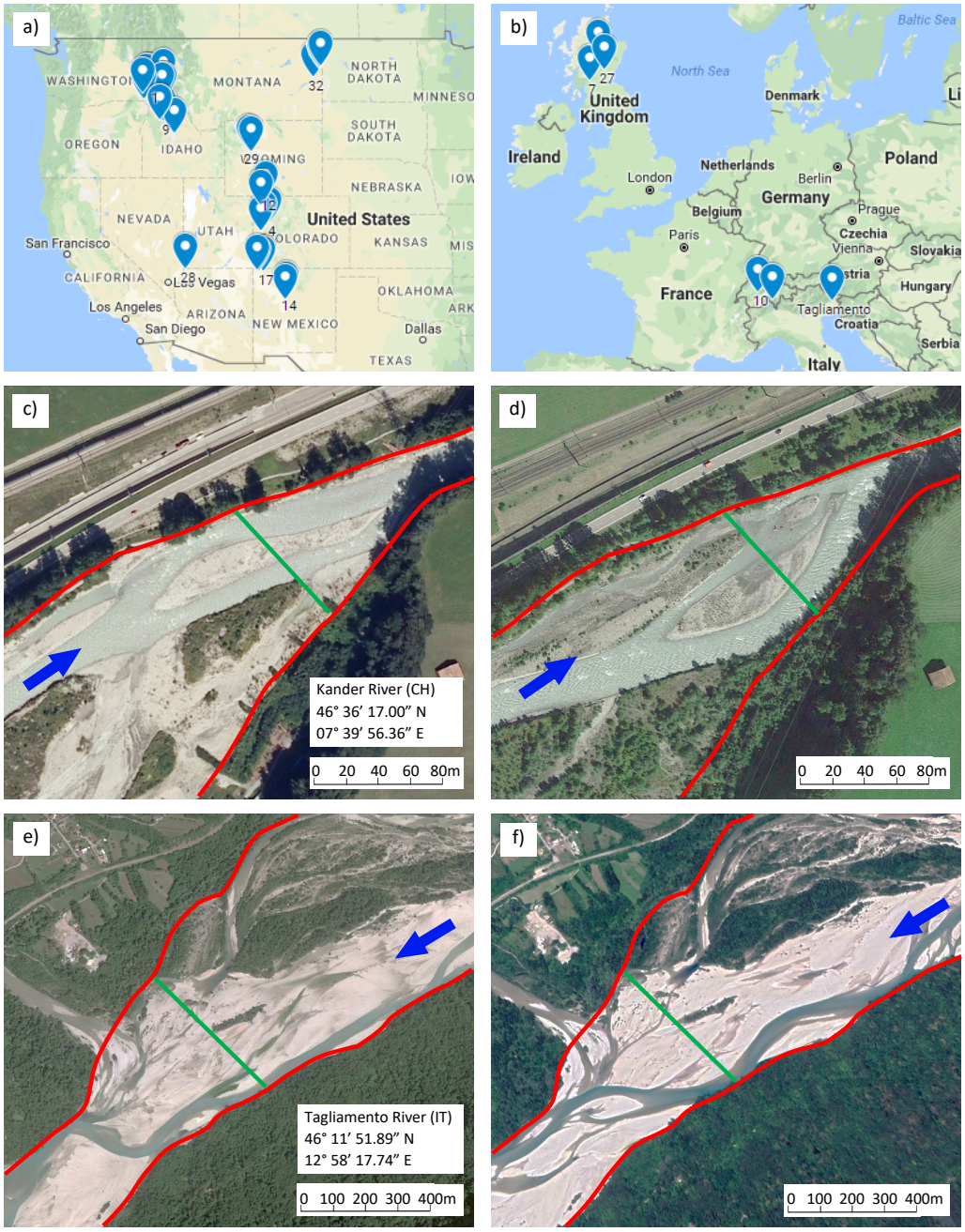

Figure 1. Convergent banks in rivers are an ubiquitous planform configuration. a,b) Worldwide location of the river reaches included in the analysis - Images from Google Earth. c) A reach of the Kander River (Switzerland) showing the presence of a vegetation front in 2009. d) The same reach of the Kander River in 2016. Although bar morphology changed, the location of the vegetation front is stable. e) A reach of the Tagliamento River (Italy) showing the presence of a vegetation front in 2016. f) The same reach of the Tagliamento River in 2018, with unchanged position of the vegetation front. Red lines highlight the converging configuration of riverbanks. Green lines show the position of the vegetation front.

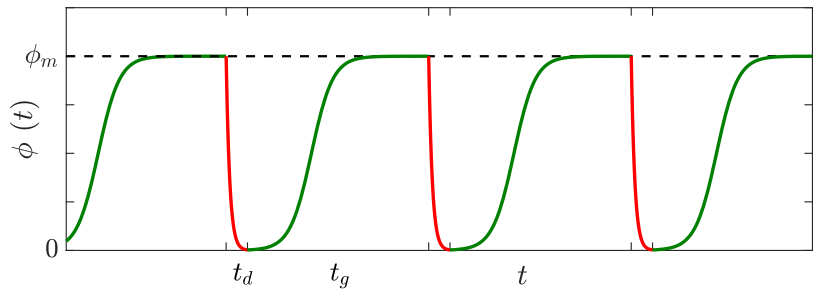

573 **Figure 2.** A possible solution to the logistic law for vegetation dynamics ((Replaced: ~~Eq.~~ replaced with:
574 Equation) (2)) when growth and decay terms are separately active. Green line represents the solution consid-
575 ering the growing term governed by α_g and t_g is its duration. Red line is the solution considering the decay
576 rate α_d only and t_d is the decay duration.

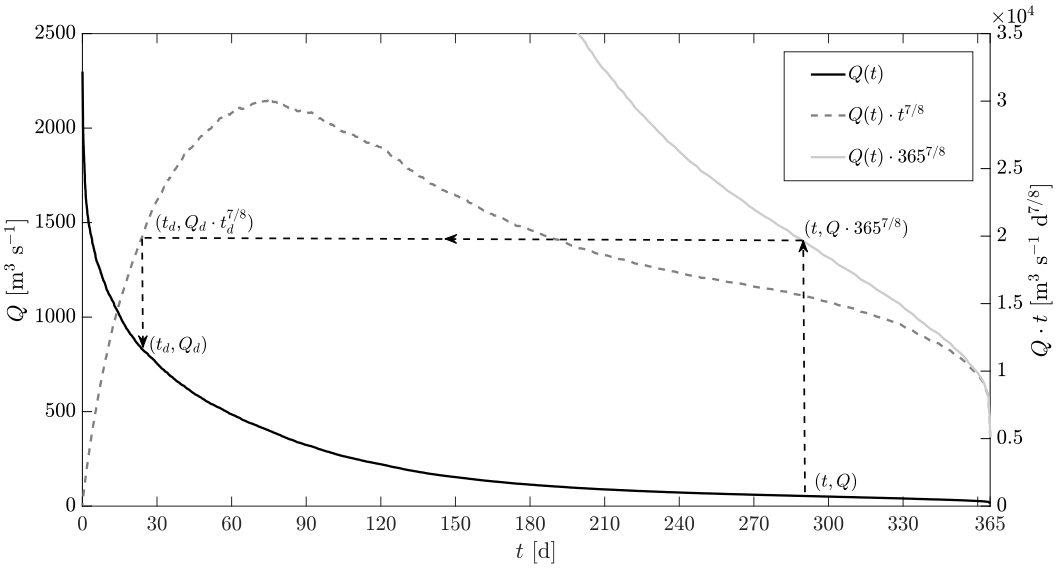

577 **Figure 3.** A common flow duration curve (continuous black line) and the associated parabolic-like shape
578 curve obtained as a result of the product by its duration time to the power of 7/8 (dashed dark-gray line).
579 Continuous light-gray curve is the flow duration curve multiplied by $365^{7/8}$. Dashed black lines show the
580 calculation of the flow discharge Q_d and its relative duration time t_d.

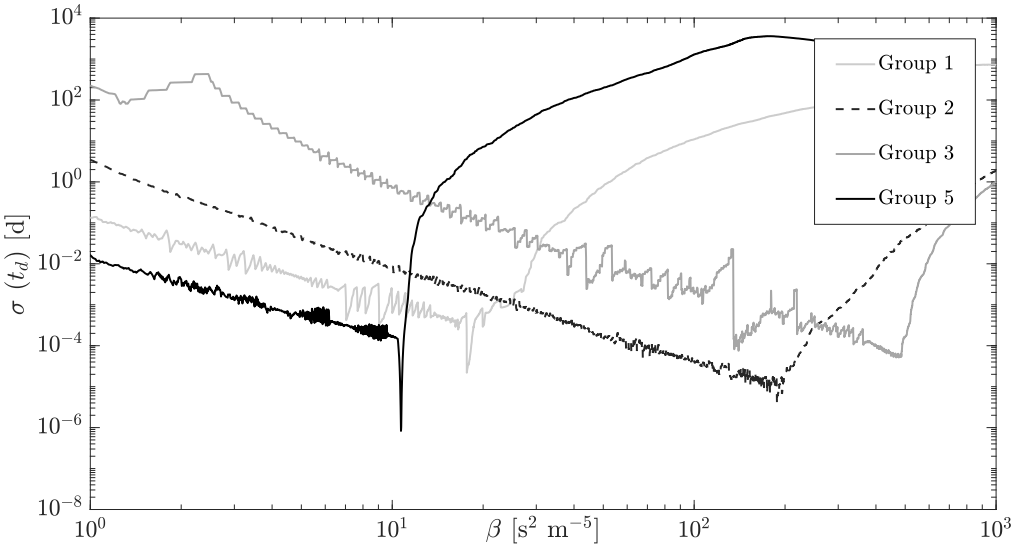

581 **Figure 4.** t_d standard deviation (σ) versus the parameter β at varying the vegetation cover properties (i.e.,
582 river group). The curves show the t_d standard deviation slowly decreasing and fast rising after having reached
583 a minimum.

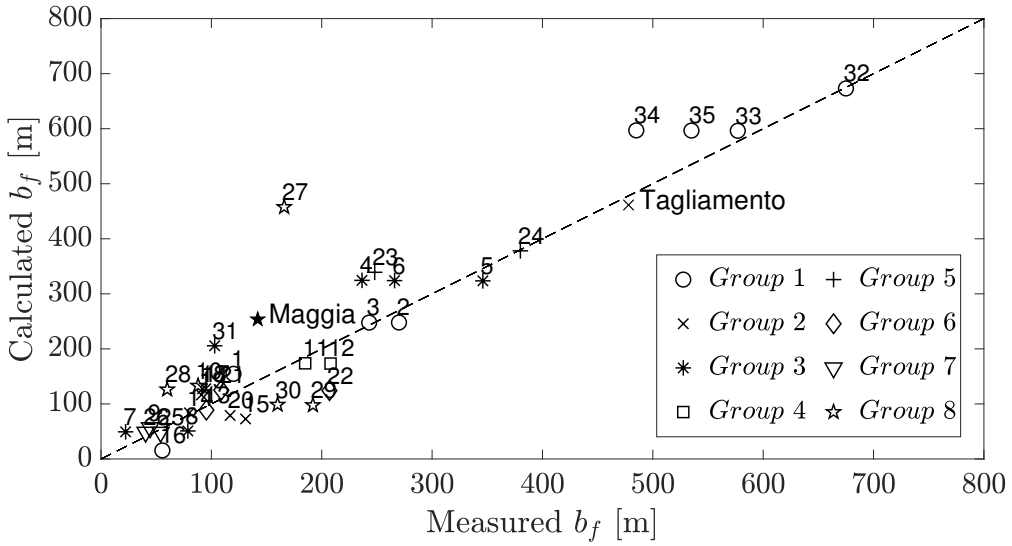

584 **Figure 5.** Comparison between measured and calculated river width at the vegetation front (b_f) for the
585 river reaches we tested, according to different vegetation cover (Group ID). The comparison for the Maggia
586 River (Group 8 - black star) and the Tagliamento River (Group 2 - black cross) is shown as validation cases.

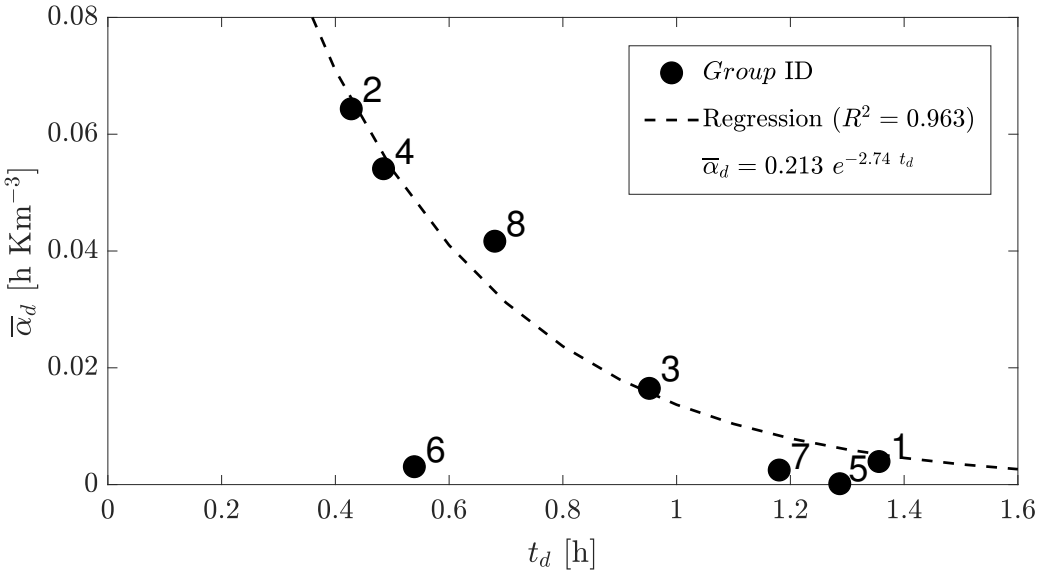

Figure 6. Average vegetation decay coefficient $\overline{\alpha}_d$ versus the characteristics time t_d in the flow duration curve controlling the biomorphological properties at the reach scale. Each vegetation cover is characterised by a particular combination of decay rate $\overline{\alpha}_d$ and temporal scale in the flow duration curve, showing that underlying interactions between hydro-morphology and vegetation govern the uprooting process at the reach scale, according to the different plant species.

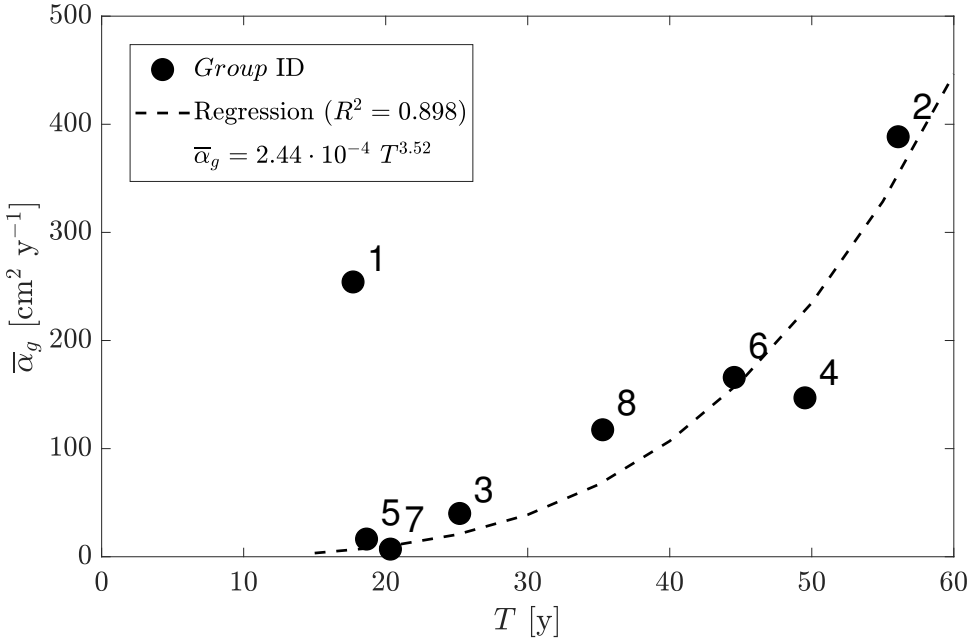

592 **Figure 7.** Average vegetation growth rate $\overline{\alpha}_g$ versus the return period T of the flow controlling the river
593 width at the reach scale. Species with higher growth rate can develop a strong root apparatus so withstand and
594 survive to higher flow discharges. Conversely, slowly growing plants are more susceptible to be uprooted even
595 for low flow events.

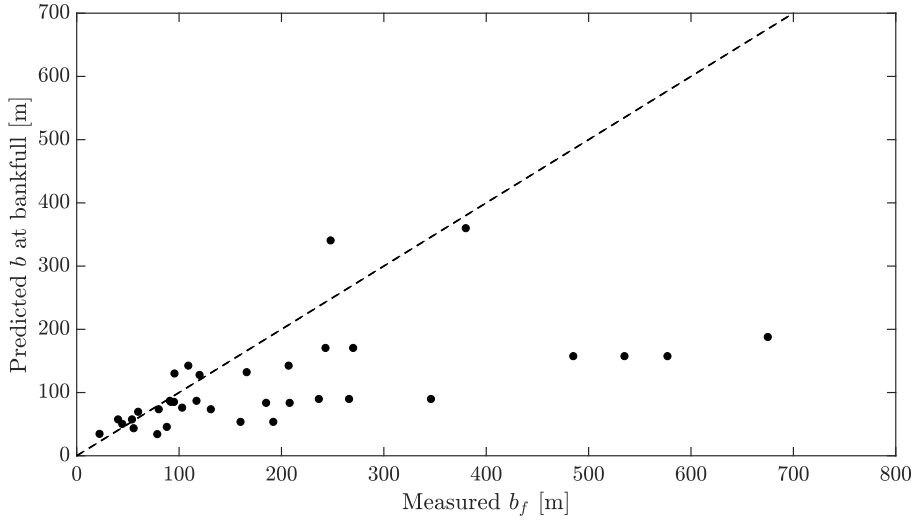

596 **Figure 8.** Comparison between measured width at the vegetation front and the bankfull width predicted
597 using Lacey's relation for the steady flow discharge Q. Agreement is good only for very small rivers whereas
598 it is lost for widths larger than approximately 150m.

			[° ’ ”]	[° ’ ”]	[m]	[‰]	[mm]	[mm]	[m^3 d^{-1}]	Species	Cover [%]	[cm^2 y^{-1}]	[10^{-3} m^{-2}]
1	1	Clearwater 1 (5)(17)(21)(22) (26)(28)(29)	46° 29’ 17.01” N	116° 15’ 41.91” W	120	1.57	58.8	114.2	200.7	Balsam poplar Other willows Sandbar willow	64% 33% 3%	79.94	35.46
	2	Clearwater 2 (5)(17)(21)(22) (26)(28)(29)	46° 31’ 16.97” N	116° 40’ 08.12” W	270	1.29	44.4	111.3	200.7	Balsam poplar Other willows Sandbar willow	64% 33% 3%	79.94	35.46
	3	Clearwater 3 (5)(17)(21)(22) (26)(28)(29)	46° 29’ 19.63” N	116° 44’ 28.74” W	243	1.29	44.4	111.3	200.7	Balsam poplar Other willows Sandbar willow	64% 33% 3%	79.94	35.46
	16	Salmon (5)(20)(21)(22)(28)(29)	44° 15’ 14.13” N	114° 41’ 00.59” W	56	3.40	104	396	12.96	Douglas fir. Sandbar willow	77% 23%	309.6	44.14
	32	Yellowstone 1 (5)(17)(18)(21) (22)(28)(29)	47° 07’ 42.86” N	104° 42’ 05.16” W	675	0.75	57	160	1382	Plains cotton. Russian olive Sandbar willow	79% 15% 6%	369.3	15.17
	33	Yellowstone 2 (5)(17)(18)(21) (22)(28)(29)	47° 30’ 14.49” N	104° 15’ 22.42” W	577	0.36	57	160	1382	Plains cotton. Russian olive Peach. willow Sandbar willow	78% 14% 5% 3%	375.6	11.56
	34	Yellowstone 3 (5)(17)(18)(21) (22)(28)(29)	47° 35’ 27.12” N	104° 12’ 36.41” W	485	0.36	57	160	1382	Plains cotton. Russian olive Peach. willow Sandbar willow	78% 14% 5% 3%	375.6	11.56
	35	Yellowstone 4 (5)(17)(18)(21) (22)(28)(29)	47° 37’ 36.64” N	104° 10’ 07.75” W	535	0.36	57	160	1382	Plains cotton. Russian olive Peach. willow Sandbar willow	78% 14% 5% 3%	375.6	11.56

Group	ID	Site[a] (Ref.)	Latitude [° ’ ”]	Longitude [° ’ ”]	B_f [m]	S [‰]	D_{50} [mm]	D_{90} [mm]	Q_s [m^3 d^{-1}]	Vegetation characteristics and parameters			
										Species	Cover [%]	$\overline{\alpha}_g$ [cm^2 y^{-1}]	$\overline{\phi}_m$ [10^{-3} m^{-2}]
2	14	Rio Grande 1 (5)(10)(17)(22) (24)(28)(29)	35° 16’ 13.96” N	106° 35’ 35.41” W	80	0.83	0.462	1.125	2247	Fremont cotton.	52%	1.4090	63.56
										Salt cedar	41%		
										Russian olive	6%		
										Sandbar willow	1%		
	15	Rio Grande 2 (5)(10)(17)(22) (24)(28)(29)	35° 05’ 53.99” N	106° 41’ 35.28” W	131	0.83	0.462	1.125	2247	Fremont cotton.	52%	444.3	63.56
										Salt cedar	41%		
										Russian olive	6%		
										Sandbar willow	1%		
	17	San Juan 1 (5)(10)(16)(17)(22)(28)	36° 43’ 57.83” N	108° 14’ 58.31” W	95	4.10	40	100	28.51	Plains cotton.	42%	1.362	50.00
										Russian olive	29%		
										Salt cedar	29%		
	18	San Juan 2 (5)(10)(16)(17)(22)(28)	36° 43’ 23.14” N	108° 18’ 53.63” W	92	4.10	40	100	28.51	Plains cotton.	42%	429.5	50.00
										Russian olive	29%		
										Salt cedar	29%		
	19	San Juan 3 (5)(10)(16)(17)(22)(28)	36° 46’ 22.16” N	108° 39’ 28.03” W	91	1.45	90	240	28.51	Salt cedar	43%	291.7	72.59
										Russian olive	36%		
										Plains cotton.	21%		
	20	San Juan 4 (5)(10)(16)(17)(22)(28)	36° 47’ 12.68” N	108° 41’ 38.69” W	117	1.45	90	240	28.51	Salt cedar	43%	291.7	72.59
										Russian olive	36%		
										Plains cotton.	21%		

[a]Numbers, when present, refer to different reaches in the same river.

List of references at the end of the table

Group	ID	Name (Ref.)	Lat [° ’ ”]	Lon [° ’ ”]	L [m]	S_0 [‰]	D_{50} [mm]	D_{84} [mm]	Q_{bf} [m^3 d^{-1}]	Species	Cover [%]	$\overline{\alpha}_g$ [cm^2 y^{-1}]	$\overline{\phi}_m$ [10^{-3} m^{-2}]
3	4	Colorado 1 (17)(20)(22)(28)(29)	39° 30’ 59.02” N	107° 50’ 27.87” W	237	2.71	58	90	247.5	Salt cedar Other willows Box elder	56% 30% 14%	38.47	129.3
	5	Colorado 2 (17)(20)(22)(28)(29)	39° 18’ 40.61” N	108° 13’ 30.36” W	346	2.71	58	90	247.5	Salt cedar Other willows Box elder	56% 30% 14%	38.47	129.3
	6	Colorado 3 (17)(20)(22)(28)(29)	39° 03’ 35.67” N	108° 26’ 36.66” W	266	2.71	58	90	247.5	Salt cedar Other willows Box elder	56% 30% 14%	38.47	129.3
	7	Endrik (11)(13)(15)(23)(25)	56° 03’ 19.78” N	004° 27’ 10.80” W	22	1.44	28.9	57.3	524.1	Goat willow Common alder Scots pine	66% 17% 17%	43.84	114.3
	8	Feshie (4)(11)(13)(15)(23)	57° 05’ 32.40” N	003° 54’ 11.34” W	79	9.62	54	90	20.82	Goat willow Common alder Scots pine	66% 17% 17%	43.84	114.3
	31	Yampa (2)(3)(5)(12)(22)(28)	40° 27’ 40.54” N	108° 25’ 29.27” W	103	1.26	34	82	359.1	Sandbar willow Box elder	82% 18%	37.53	124.2
4	11	Little Snake 1 (2)(5)(14)(17)(22)(28)	40° 35’ 16.76” N	108° 23’ 02.08” W	185	1.23	48.5	87.0	857.5	Other willows Russian olive	60% 40%	147.0	97.40
	12	Little Snake 2 (2)(5)(14)(17)(22)(28)	40° 53’ 06.27” N	108° 07’ 29.89” W	208	1.23	48.5	87.0	857.5	Other willows Russian olive	60% 40%	147.0	97.40
5	23	Snake 1 (5)(20)(21)(22)(28)	46° 02’ 21.87” N	116° 55’ 48.00” W	248	1.16	54.0	90.0	172.8	Netl. hackberry	100%	163.7	77.33
	24	Snake 2 (5)(20)(21)(22)(28)	46° 18’ 26.35” N	117° 00’ 28.75” W	380	0.47	54.0	90.0	172.8	Netl. hackberry	100%	163.7	77.33

Table 2. Summary of collected data for the 35 river cross-sections. Group refers to similar characteristics of vegetation cover.

Group	ID	Site[a] (Ref.)	Latitude [° ’ ”]	Longitude [° ’ ”]	B_f [m]	S [‰]	D_{50} [mm]	D_{90} [mm]	Q_s [m^3 d^{-1}]	Vegetation characteristics and parameters			
										Species	Cover [%]	$\overline{\alpha}_g$ [cm^2 y^{-1}]	$\overline{\phi}_m$ [10^{-3} m^{-2}]
6	13	NF Clearwater (6)(7)(10)(19)(22)	46° 45’ 04.96” N	115° 31’ 12.53” W	96	7.94	95	282	26.87	Western cedar	79%	163.7	35.11
										Box elder	13%		
										Other willows	8%		
	21	Selway 1 (5)(12)(17)(20)(21)(22)(27)(28)(29)	46° 04’ 57.73” N	115° 25’ 19.69” W	109	2.60	24	131	70.50	Western cedar	59%	166.8	18.40
										Ponderosa pine	22%		
										Other willows	19%		
	22	Selway 2 (5)(12)(17)(20)(21)(22)(27)(28)(29)	46° 05’ 29.02” N	115° 32’ 15.49” W	207	2.60	24	131	70.50	Western cedar	59%	166.8	18.40
										Ponderosa pine	22%		
										Other willows	19%		
7	9	Johnson (5)(20)(21)(22)(28)	44° 52’ 33.17” N	115° 30’ 26.12” W	45	5.02	190	430	0.691	Grey alder	57%	70.64	351.9
										Red osier dogw.	43%		
	25	SF Salmon 1 (5)(20)(21)(22)(28)	44° 57’ 08.84” N	115° 44’ 07.69” W	54	2.50	38	113	34.56	Grey alder	57%	70.64	351.9
										Red osier dogw.	43%		
	26	SF Salmon 2 (5)(20)(21)(22)(28)	44° 57’ 03.45” N	115° 44’ 03.38” W	40	2.50	38	113	34.56	Grey alder	57%	70.64	351.9
										Red osier dogw.	43%		

[a]Numbers, when present, refer to different reaches in the same river.

List of references at the end of the table

Table 2. Summary of collected data for the 35 river cross-sections. Group refers to similar characteristics of vegetation cover.

Group	ID	Site[a] (Ref.)	Latitude [° ’ ”]	Longitude [° ’ ”]	B_f [m]	S [‰]	D_{50} [mm]	D_{90} [mm]	Q_s [m^3 d^{-1}]	Vegetation characteristics and parameters Species	Cover [%]	$\overline{\alpha}_g$ [cm^2 y^{-1}]	$\overline{\phi}_m$ [10^{-3} m^{-2}]
8	10	Kander (6)(7)(10)(19)(22)	46° 36’ 17.00” N	007° 39’ 56.36” E	88	13.3	76	287	3654	Norway spruce	46%	233.4	48.35
										Scots pine	31%		
										Grey alder	23%		
	27	Tay (1)(8)(9)(11)(22)(23)	56° 29’ 16.19” N	003° 25’ 35.11” W	166	2.19	1.14	5	153.2	Common alder	40%	59.60	49.53
										Downy birch	40%		
										Scots pine	20%		
	28	Virgin (5)(20)(21)(22)(28)	36° 53’ 33.21” N	113° 55’ 09.95” W	27	2.86	25	75	34.56	Salt cedar	62%	219.8	95.28
										Fremont cotton.	23%		
										Black willow	15%		
	29	Wind 1 (5)(20)(22)(28)	43° 25’ 09.62” N	109° 19’ 56.54” W	192	3.34	22	75	267.8	Water birch	48%	41.31	67.27
										Spruce	36%		
										Narrow. cotton.	16%		
	30	Wind 2 (5)(20)(22)(28)	43° 18’ 57.13” N	109° 08’ 00.02” W	105	3.34	22	75	267.8	Water birch	48%	41.31	67.27
										Spruce	36%		
										Narrow. cotton.	16%		

[a]Numbers, when present, refer to different reaches in the same river

(1) *Al-Ansari and McManus* [1979]; (2) *Andrews* [1980]; (3) *Andrews* [1984]; (4) *Ashworth and Ferguson* [1989]; (5) *Auble et al.* [2012]; (6) *BAFU Data* [2017]; (7) *BAFU GeoData* [2017];

(8) *Bates et al.* [2004]; (9) *Bryant and Gilvear* [1999]; (10) *Charlton et al.* [1978]; (11) *Claessens et al.* [2010]; (12) *Elliott and Anders* [2004]; (13) *Enescu et al.* [2016]; (14) *FLO Engineering* [1994];

(15) *Gilvear et al.* [2000]; (16) *Heins et al.* [2004]; (17) *Hoag* [2005]; (18) *Holnbeck* [2005]; (19) *Jud* [2009]; (20) *Mueller et al.* [2005]; (21) *Mueller and Pitlick* [2013]; (22) *Little and Viereck* [1971];

(23) *National River Flow Archive* [2017]; (24) *Novak* [2006]; (25) *Piedra* [2010]; (26) *Sharma and Parton* [2007]; (27) *Smith* [1999]; (28) *Water Data for the Nation* [2017]; (29) *Warner and Hendrix* [1984]